Available online at www.sciencedirect.com

ScienceDirect

Microelectronics Reliability 48 (2008) 763–772

MICROELECTRONICS RELIABILITY

www.elsevier.com/locate/microrel

Comparison of thermo-mechanical behavior of lead-free copper and tin–lead column grid array packages

S.B. Park *, Rahul Joshi

Department of Mechanical Engineering, State University of New York at Binghamton, Binghamton, NY 13902, United States

Received 22 September 2007; received in revised form 8 December 2007
Available online 21 February 2008

Abstract

Thermo-mechanical behavior of the lead (Pb)-free ceramic copper column grid array (CuCGA) package under accelerated thermal cycling is characterized and compared with the conventional tin–lead (Sn–Pb) ceramic column grid array (CCGA). In situ thermal deformations of the highest DNP (distance to neutral point) copper column is measured for an initial isothermal loading of $\Delta T = -75$ °C and subsequent accelerated thermal cycling of −40 °C to +125 °C. The deformed shape of the column and the distribution of inelastic strains are measured from the displacement fields. The dominant deformation mode is bending of the column due to thermal expansion mismatch between the module and the printed circuit board (PCB). The results are compared with those of tin–lead CCGA tested under similar conditions. Unlike tin–lead columns, where the failure occurs at the column near the top of the solder fillet and through the thickness of the column, in the CuCGA, the failure is found to occur first in the solder fillet at the solder/copper column interface and the crack propagates along the periphery of the copper column. The accumulated plastic deformation per cycle is larger in tin–lead columns compared to the copper columns. A deformation mechanism is provided to explain the nature of this failure.
© 2008 Elsevier Ltd. All rights reserved.

1. Introduction

The worldwide ban on lead containing products has made the microelectronics industry incorporate 'Lead (Pb)-Free' alternatives in its components, solders and processes. The Pb-free CuCGA was developed by IBM [1] to replace conventional Pb-containing CCGA packages. Like the CCGA, the CuCGA offers a high reliability packaging solution without compromising on the electrical and thermal performances. The CuCGA consists of an annealed and tin-plated copper column in place of a high lead (Sn/90Pb) solder column and Pb-free Sn/3.9Ag/0.6Cu (SAC) solder fillets in place of eutectic solder fillets [2]. The ceramic substrate side solder fillet is the higher melting Sn/18Ag solder to maintain the packaging hierarchy. The copper column of the package used in this study, is thinner and taller (2.46 mm long, 0.25 mm in diameter) than the Sn/90Pb solder column (2.2 mm long, 0.57 mm in diameter). This is to compensate for the inherent higher stiffness of the copper columns as compared to that of the Sn–Pb columns. The column dimensions affect the electrical and mechanical performance such that shorter in length, larger in diameter columns improve the electrical performance but reduce the fatigue life and the converse improves the fatigue life at the cost of electrical performance [3]. Accordingly, through modeling and testing at IBM, the copper column dimensions are selected to provide comparable or superior electrical performance to similar tin–lead packages.

Several experimental and numerical studies have been conducted on Sn–Pb CCGAs. Parametric studies were performed to understand the thermo mechanical behavior of Sn–Pb CCGA and validated by experiments [4]. More recently, the vibration induced solder joint failure of the Sn–Pb CCGA was also evaluated [5]. In a recent study [6], Sn–Pb CCGA packages were thermally cycled and its thermo-mechanical deformation mechanism was identified and quantified by the moiré interferometer. The tin–lead

* Corresponding author. Tel.: +1 607 777 3415.
E-mail address: sbpark@binghamton.edu (S.B. Park).

0026-2714/$ - see front matter © 2008 Elsevier Ltd. All rights reserved.
doi:10.1016/j.microrel.2007.12.008

columns experienced high bending strains in the solder column near the top of the solder fillets. The plastic strain accumulated during thermal cycling led to the fracture of the high lead solder column. In addition to the Sn–Pb and the Pb-free CCGA, some 'Pb-reduced' CCGAs are also present. These are manufactured in order to bridge the gap between Sn–Pb and Pb-free CCGA and to effect a smoother transition to Pb-free. This particular type uses Pb-free Sn/3.9Ag/0.6Cu (SAC) solder paste on Pb-free PCBs. However, the column continues to be the Sn/90Pb high lead solder column. The reliability of this particular class of CCGA was evaluated experimentally [7]. Using numerical modeling, the time history creep strain energy density of the solder columns with Pb-containing and Pb-free solder pastes were evaluated under thermal cycling that was then verified experimentally [8].

The present experimental study uses a high sensitivity moiré interferometer [9] to analyze the thermo-mechanical behavior of the 1657 I/O, 42.5 mm, CuCGA package. In situ thermal deformations of the highest DNP (distance to neutral point) column are measured for an initial isothermal loading of $\Delta T = -75\,°C$ (corresponding to the epoxy replication temperature of 100 °C and room temperature of 25 °C) and subsequent accelerated thermal cycling of −40 °C to +125 °C. Thermal expansion mismatch between the module and the PCB causes bending in the column. The deformed shape of the column and the distribution of inelastic strains are calculated from the displacement fields. The results are compared with those of Sn–Pb CCGA tested under similar conditions [6].

2. Moiré interferometry and experimental setup

Moiré interferometry is a whole field optical method to measure in-plane deformation with a high in-plane displacement measurement sensitivity of 0.417 μm per fringe order. In this method, a high frequency (1200 lines/mm) crossed-line diffraction grating is applied to the specimen surface that reveals the deformation of the specimen with high fidelity. The interaction of the deformed specimen grating with the virtual reference grating of the interferometer creates the moiré fringe pattern, which is viewed by the imaging system. The fringes obtained are contours of in-plane horizontal (U) and in-plane vertical (V) displacement. Displacement and strain information are extracted from these fringe patterns by using mathematical relations [10].

2.1. CuCGA Sample preparation

The CuCGA package is a 42.5 mm square module assembled with 1657 (41 × 41) column interconnections. Fig. 1 shows the dimensions and materials used in the Sn–Pb CCGA and Pb-free CuCGA assemblies. The CuCGA package specifications are listed in Table 1. The specimen was prepared by cutting a strip of central rows of the solder columns from the assembly and the cross-section was polished flat. The strip cross-section of the CuCGA was employed to facilitate comparison of results of the present study with those of the Sn–Pb CCGA from [6].

A high frequency cross-line grating from an ultra low expansion (ULE) grating mold was then replicated onto the flat, polished cross-section of the specimen at elevated temperature creating the specimen grating. The replication process consisted of preheating and soaking the specimen at elevated temperature, attaching the ULE grating mold to the specimen using a thin layer of high temperature epoxy, and finally separating the specimen from the ULE grating mold after curing of the epoxy. In this study, a high temperature epoxy [11] with a cure temperature of 100 °C was used for replication. This temperature can be treated as the reference temperature or undeformed state. When the specimen was brought back to room temperature, it possessed the deformation signature via the deformation

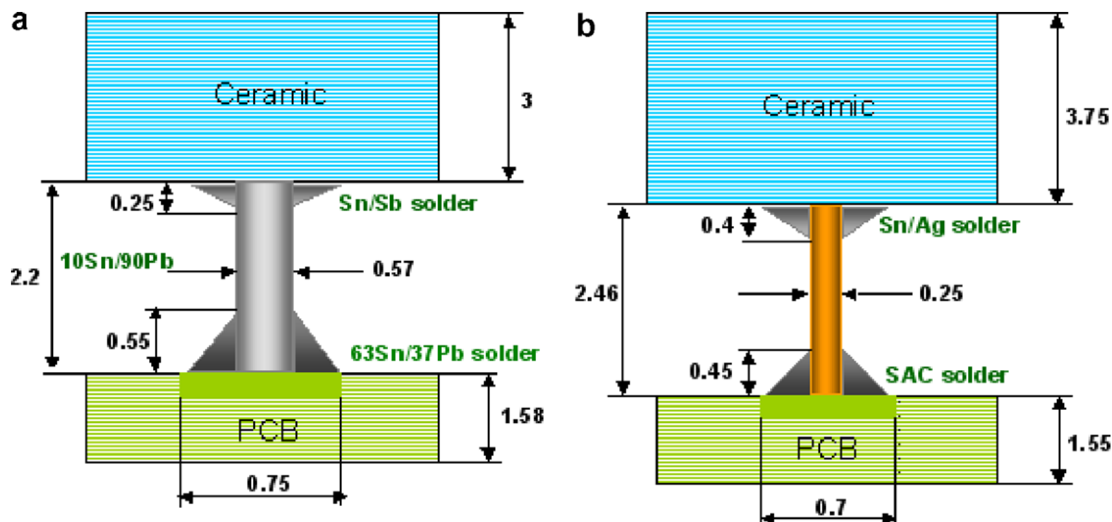

Fig. 1. Schematic diagram of (a) Sn–Pb CCGA and (b) CuCGA package (All dimensions in mm).

Table 1
CuCGA package details

Lead-free CuCGA Package		
Ceramic module		
Substrate material		White Alumina
Dimension		42.5 × 42.5 and 3.75 mm thick
Assembly		
Column		Tin plated, annealed Copper
Dimension		0.25 mm diameter; 2.46 mm height; 1.0 mm pitch
Array		41 × 41 (1657 total) with depopulated corners
Solder fillets		
Material:	Top	Sn/18Ag
	Bottom	Sn/3.9Ag/0.6Cu (SAC)
Pad		
Material		Copper; 0.7 mm diameter
PCB		
Material		FR-4 with OSP surface finish; 1.55 mm thickness

of the grating. Now when the specimen grating was made to interact with the virtual reference grating at room temperature, the moiré fringe pattern thus generated, provided the displacement the specimen had undergone due to the isothermal loading.

2.2. Experimental procedure

Two CuCGA samples were prepared. The first sample was subjected only to an isothermal load of $\Delta T = -60$ °C so as to compare column compliance data with tin–lead CCGA data available in the literature [6]. Fig. 2 shows the U field deformation of the left half of a CuCGA sample for an isothermal load of $\Delta T = -60$ °C. The near vertical fringes in the PCB and ceramic substrate indicate that there was little bending of the package. It can also be noted that the fringe density of the column increased from the centre (DNP = 0) to the outer column. Therefore, bending (flexure) of columns was the major deformation mode with minimal amount of package warpage. The outermost column (max DNP) experienced highest shear strains and hence the focus was on deformation and strain analysis of this column.

The second sample was subjected to an isothermal load of $\Delta T = -75$ °C. Fig. 3a shows the total deformation U and V fields of the outermost column, while Fig. 3b shows the same with carrier fringes of rotation applied for the convenience of deformation analysis [6,10]. The fringe patterns indicate the fillet regions as areas of strain concentration.

The total deformation information contained in Fig. 3 consists of the mechanical and thermal deformations. In order to obtain only the stress-induced deformation, carrier fringes of extension were applied to the center column (DNP = 0), to optically subtract off the free thermal contraction [6,10]. The resulting fringe patterns of the outermost column are shown in Fig. 4.

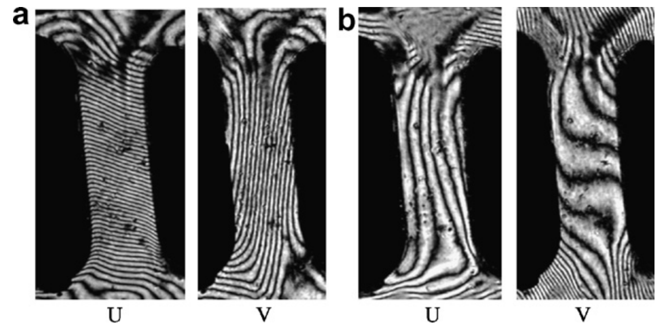

Fig. 3. Outermost column: (a) total displacements due to isothermal loading ($\Delta T = -75$ °C) and (b) the same with carrier fringes of rotation.

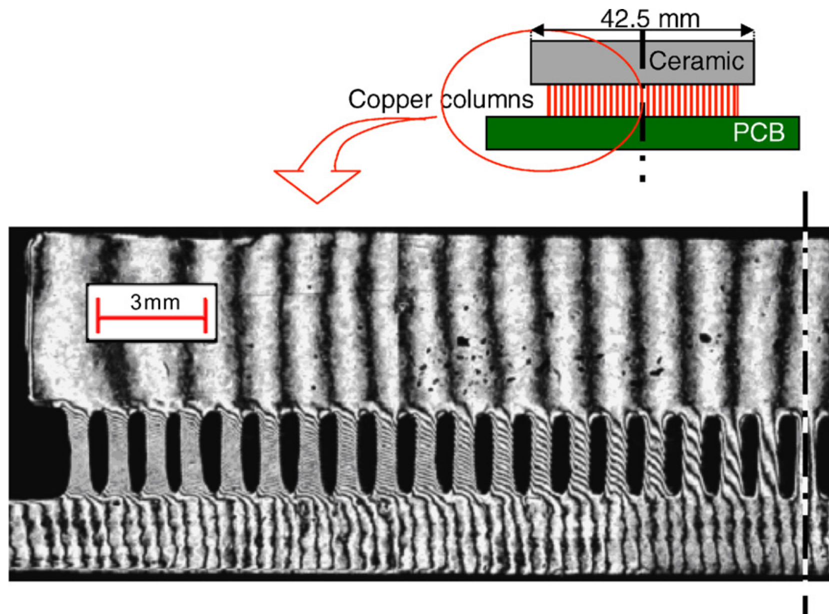

Fig. 2. U-field displacement of the left half of the CuCGA module subjected to an isothermal load of $\Delta T = -60$ °C.

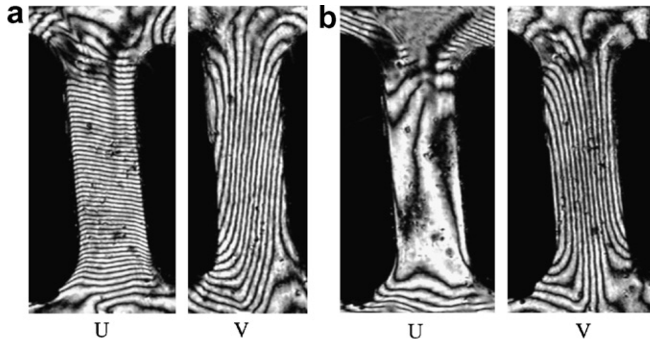

Fig. 4. Outermost column with carrier fringe extension: (a) stress induced displacements due to isothermal loading ($\Delta T = -75$ °C) and (b) the same with carrier fringes of rotation.

Note that, carrier fringes of rotation results in the same deformation signature and only helps in fringe analysis. It is employed here to simplify the fringe analysis. In the mean time, the carrier fringe extension changes its information by subtracting or adding deformation. It is a common practice applying the carrier fringe extension to deduct the free thermal expansion from its total resultant deformation.

2.3. Accelerated thermal cycling

Subsequent to the isothermal loading, thermal cycling of the same specimen was carried out as per the temperature profile of Fig. 5 to understand the deformation of the columns and to record the accumulated plastic strains per cycle. Fig. 6 shows the total deformation in U and V fields of the outermost column after 8 cycles and Fig. 7 shows the same after 16 cycles. These images were obtained after thermal cycling. In case of in situ measurements during thermal cycling, better quality images are obtained by switching off the oven momentarily to record the image to avoid the undesirable effect of unsteady fringes due to vibration.

3. Results

3.1. Compliance of columns

The relative horizontal displacements between the top and bottom of the columns of the CuCGA specimen from

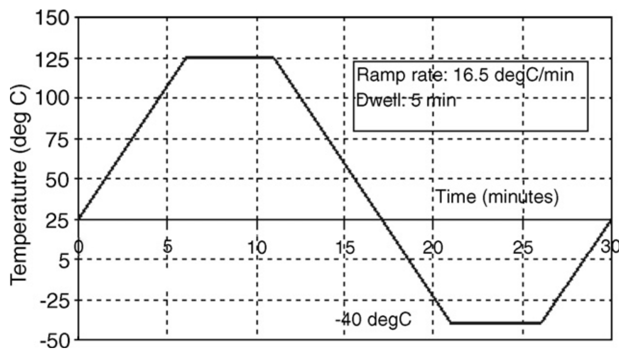

Fig. 5. Temperature profile of the thermal cycle.

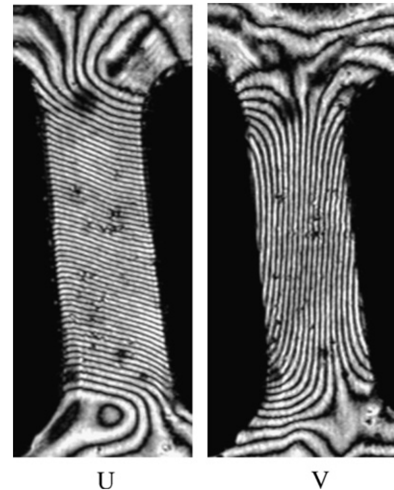

Fig. 6. Outermost column – total displacements after 8 thermal cycles (−40 °C to +125 °C).

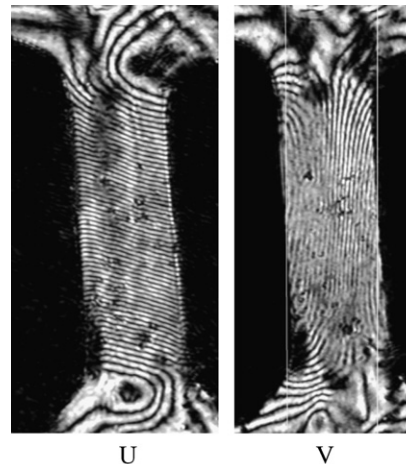

Fig. 7. Outermost column – total displacements after 16 thermal cycles (−40 °C to +125 °C).

the center of the package to the outermost column are presented in Fig. 8. They are compared with similar data for the similar-sized (42.5 mm) tin–lead CCGA package (33 × 33 column array) [6]. The package comparisons between the CuCGA and CCGA are provided in Fig. 1. It can be seen that the deformation increases from the center to the outermost column linearly. Even though the module sizes for both packages are similar, the CuCGA, owing to its finer pitch (1 mm) accommodates more number of columns compared to tin–lead CCGA which has a pitch of 1.27 mm. However, it is interesting to note that the outermost column of the CuCGA specimen (20th column from the center), and the 16th solder column of the tin–lead CCGA specimen have the same horizontal displacements. It suggests that either the packages have similar global stiffness of the column interconnects or the column stiffness is insignificant relative to the ceramic/PCB moduli. In the latter case, the columns may be treated

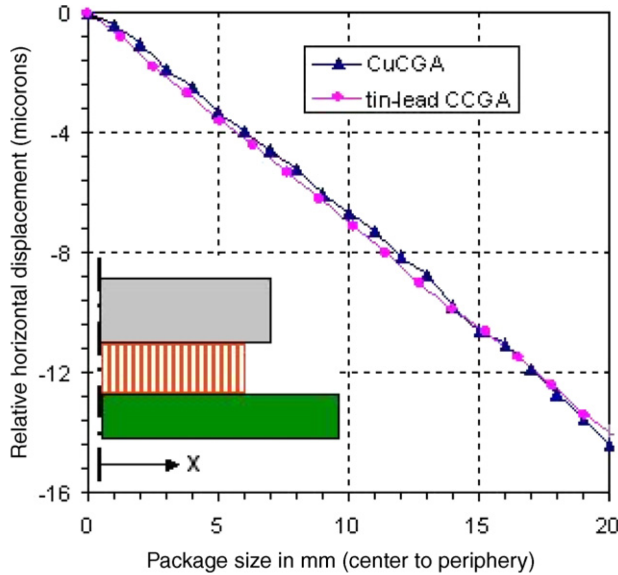

Fig. 8. Relative horizontal displacements across the height of the solder columns ($\Delta T = -60$ °C).

as being subjected to displacement loading dictated by thermal expansions of ceramic and PCB. Similar result was also noted for Sn–Pb columns with Pb-free solder pastes [7]. Perkins and Sitaraman [4] also observed through their parametric study that for the same package size, on reducing the pitch from 1.27 mm to 1 mm, causes no significant change in the fatigue life. As the columns deform, the stiffness, which is governed by the modulus, length and diameter of the column, is responsible for generating bending moments. These contribute to the strains that are imparted to the solder fillets and that get accumulated with thermal excursions. As the copper columns of the package used in this study are thinner and taller (2.46 mm long, 0.25 mm in diameter) than the tin–lead columns (2.2 mm long, 0.57 mm in diameter) as seen in Fig. 9, the copper columns have higher flexibility than their tin–lead counterparts. This is explained below. For a rough estimate of the relative stiffness of the copper and SnPb columns, the simple beam formula with fixed ends can be used as shown below.

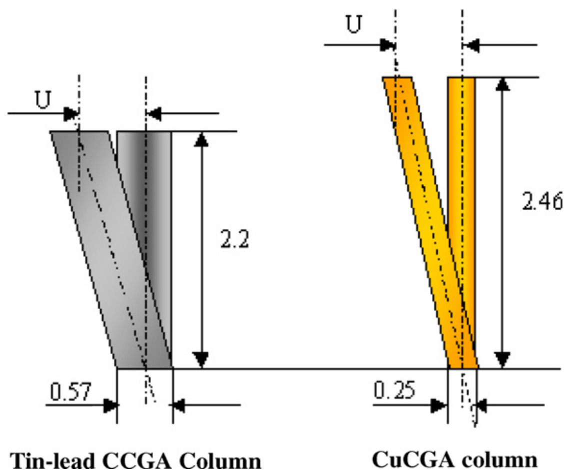

Fig. 9. Schematic of copper and tin–lead column deformation at the highest DNP column.

For such a beam element, force (F) and moment (M) can be written as Eqs. (1) and (2).

$$F = \frac{12EI}{l^3}x \quad (1)$$

$$M = \frac{Fl}{2} = \frac{6EI}{l^2}x \quad (2)$$

where E is Young's modulus (N/mm^2), d is column diameter (mm), I is moment of inertia ($\pi d^4/64$ mm^4) and l is column length (mm).

Hence, flexural stiffness (k) of the column can be given by:

$$k = F/x \quad \text{or} \quad k = \frac{12\pi}{64}\frac{Ed^4}{l^3} \quad (3)$$

Using Young's moduli for Cu column and Sn/90Pb column as 110 GPa and 21.8 GPa, respectively, their stiffness can be written as $k_{\mathrm{Cu}} = 17$ N/mm and $k_{\mathrm{SnPb}} = 127.42$ N/mm. The copper column is approximately 7 times more flexible than 10Sn/90Pb solder column and therefore the moment generated would be far less for the copper column. Due to higher yield strength of copper, the copper column would undergo less plastic deformation than the solder material suggesting the reason for the difference in failure mechanisms.

3.2. Deformed shape analysis

The overall shape change of the column induced by thermal loading can be obtained from the total displacement fields shown in Figs. 3 and 6. These figures were constructed by superimposing a grid over the horizontal in-plane displacement (U) and vertical in-plane displacement (V) fringe patterns to form a coordinate system. The displacements (U and V) are then evaluated at each nodal point along the left and right edges of the column. Figs. 10 and 11 show the deformation of the outermost column after isothermal loading and after 8 thermal cycles, respectively. Note that the deformations shown in the figures are obtained after multiplying the actual values by 20 for visualization.

In the plots, the bases of the initial and deformed shape are set together so that the relative deformation can be gauged. It becomes clear from the deformed shape (S-shaped) that the columns experience bending. Although the amount of relative horizontal deformation between the top and bottom of a column are similar for the two loading cases (i.e. isothermal and cyclic loading), the deformed shapes are noticeably changed. They are behaving similar to those observed in the case of tin–lead solder columns where the shape change is more significant at the top of solder fillets [6].

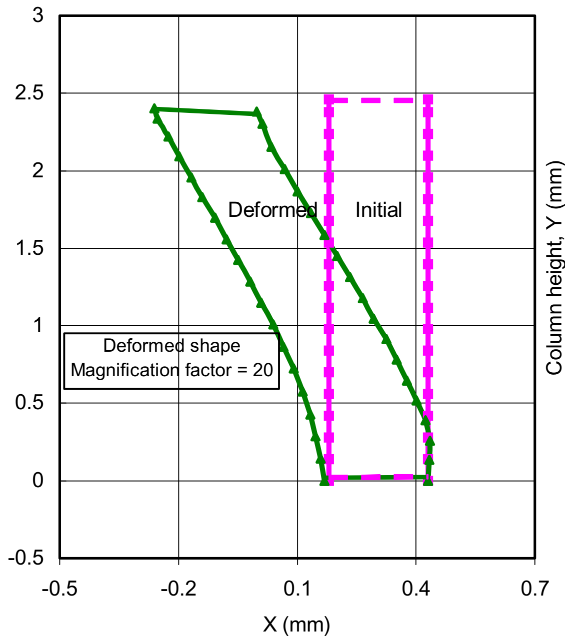

Fig. 10. Deformed shape of outermost column at room temperature due to isothermal loading ($\Delta T = -75$ °C).

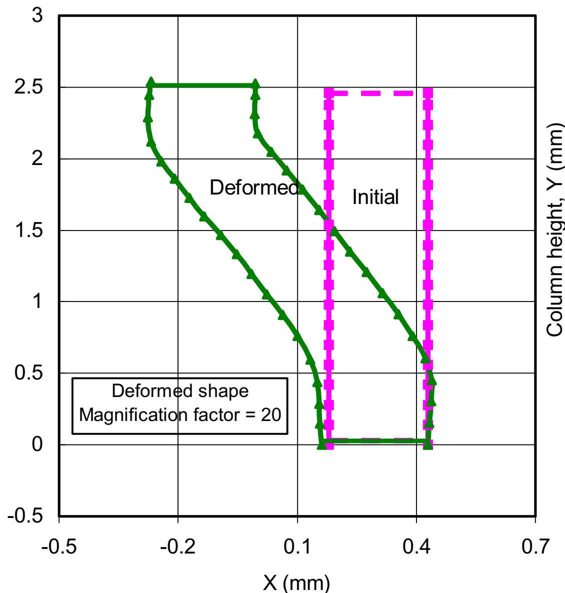

Fig. 11. Deformed shape of outermost column at room temperature after 8 thermal cycles (−40 °C to +125 °C).

The horizontal displacements of the outermost column are plotted along its centerline for various thermal cycles in Fig. 12. This plot provides information on the progressive horizontal deformation with increasing number of thermal cycles. The S-shaped bending is evident. There is little bending in the middle portion of the column as compared to the upper and lower portions that are enclosed in the solder fillets. Significant horizontal deformations are seen at the top of the upper and lower solder fillets.

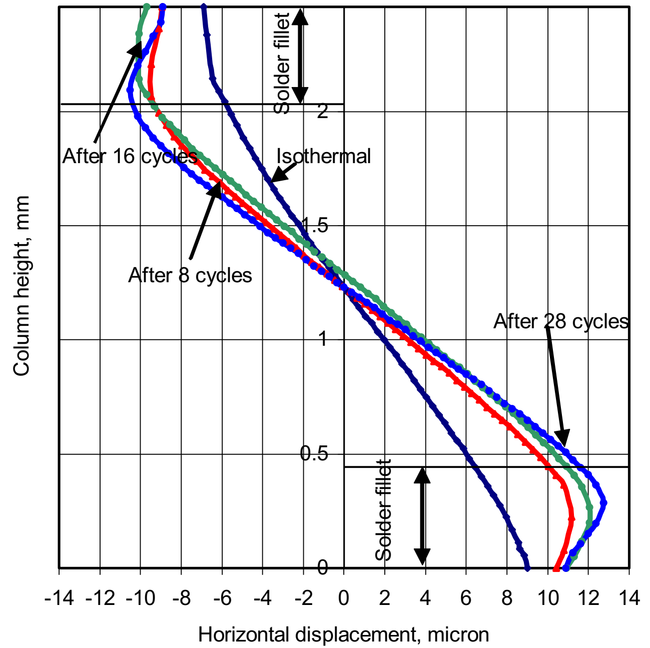

Fig. 12. Distribution of horizontal distribution along the centerline of the column.

3.3. Bending strain distribution

The deformation is mainly due to bending of the column. To analyze the amount of bending, the normal strain ε_y was extracted from the V field of Figs. 3, 6 and 7. This bending strain distribution along the left and right side of the maximum DNP column is plotted in Fig. 13 for isothermal, 8 and 16 cycles. For all the cases, the strain distributions are symmetric about the middle of the column. Moreover, the strain distributions on the left edge show a tensile nature on the upper side of the column and compressive towards the lower side and vice versa for the right edge of the column. This can be attributed to the deformed shape after thermal cycles. These results can be predicted intuitively from Fig. 12.

For the isothermal case, large tensile strains occur in the Sn/Ag solder fillet region along the left edge. The largest compressive strain occurred just above the top of the SAC solder fillet.

The post 8-cycle strain plot shows a clearly defined maximum tensile strain (+1.5%) at the top and a compressive strain (−0.74%) near the SAC solder fillet along the left edge of the column. Compressive strain (−0.34%) occurs near the Sn/Ag solder fillet and a tensile strain (+0.34%) near the SAC solder fillet along the right side of column. These figures are comparable to tin–lead case (+1% maximum tensile, −0.5% maximum compressive occurring at solder fillets) with just 4 thermal cycles.

The strain distributions after 16 thermal cycles showed marginal increase in strain for its peak value compared to 8 thermal cycles at the SAC solder fillet. However, the zone of plastic strain accumulation is generally broadened. In all

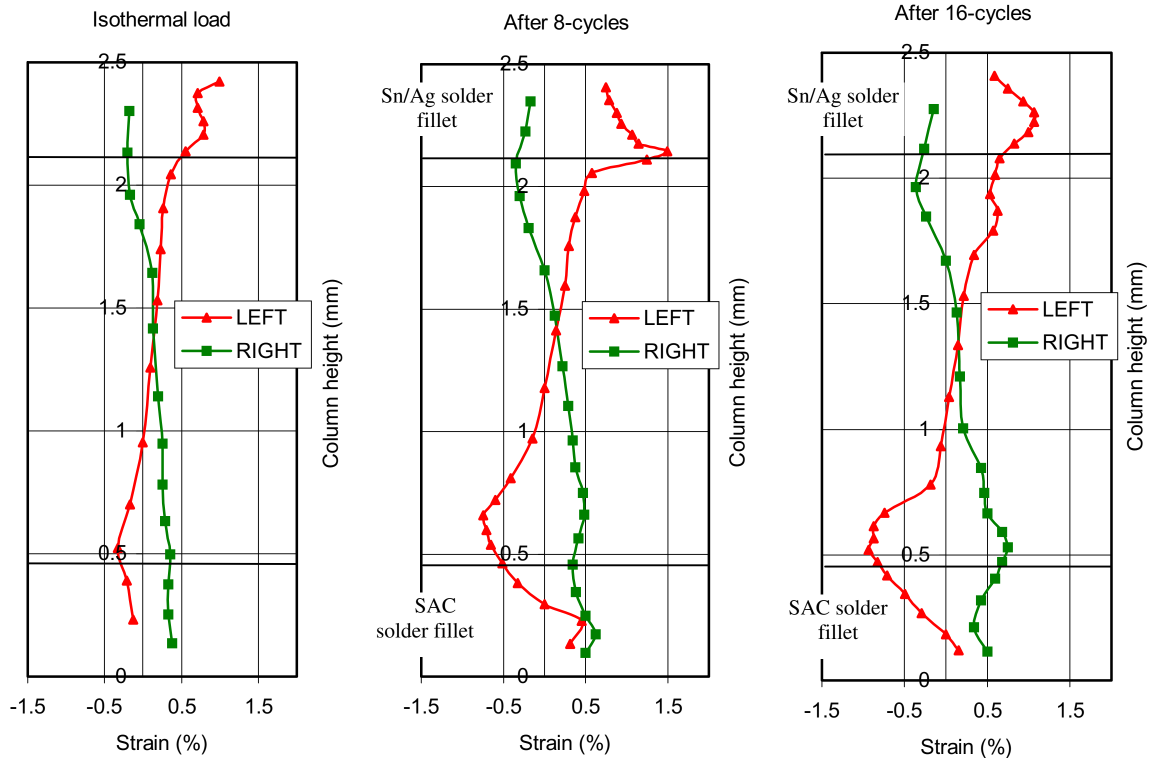

Fig. 13. Bending strain distribution along the left and right edges of outermost column.

three plots, the location of maximum strains is near the tops of the solder fillets. This is in good agreement with prior studies [4,6,7].

Accumulated plastic deformation during thermal cycles can be obtained by subtracting the deformation due to isothermal loading from the deformation after the thermal cycles. These inelastic strains are plotted in Fig. 14 for the left and right edges of the column. The plastic strain accumulated is larger near the top of the fillets. At the SAC solder fillet, the maximum plastic compressive strain increased from −0.97% (after 8 cycles) to −1.26% (after 16 cycles). Thus the plastic strain accumulated at the SAC solder fillet of the CuCGA is −0.29% over eight thermal cycles. In the tin–lead CCGA case, the maximum plastic compressive strain at the eutectic solder fillet increased from –0.45% (after 2 cycles) to −0.85% (after 4 cycles) [6]. Thus the plastic strain accumulated at the eutectic solder fillet of the Sn–Pb CCGA is −0.4% over two thermal cycles. Obviously, the maximum plastic strains accumulated per cycle are larger in the case of Sn–Pb CCGA than in the Pb-free CuCGA.

As is obvious from the bending strain distribution, the ends of the solder fillets are regions of strain concentration. The strain distribution along the column height would have been much smoother in the absence of the fillets. Solder fillet geometry is also one of the key factors governing the nature of failure. For the CuCGA, reducing the solder volume will result in shorter fillet height and it can have a detrimental effect, as the fillet may not withstand the ratcheting force (repeated reversal of loading) due to column bending. Increasing the solder volume may lead to increased chances of solder bridging during reflow and ultimately need costly rework [12]. Moreover, too much solder will decrease the effective flexible length of the column. Therefore, it is necessary to understand the effect of both the Sn/Ag and the SAC solder fillet geometries on the overall thermo-mechanical behavior of the column assembly. Optimization of the solder fillet geometry should be undertaken by numerical parametric studies.

4. Deformation mechanism

Based on the results of the deformed shape and bending strains from the present experimental study along with failure data for CuCGA [2], a possible deformation mechanism is suggested in Fig. 15 for the outermost column as an example. The Sn/Ag solder fillet on the ceramic side and SAC solder fillet on the board side holds the copper column. Assume the column to be straight (no initial deformation) at room temperature (Fig. 15a). On heating to an elevated temperature the lower part of the assembly expands more than the upper part owing to the higher CTE of the PCB (Fig. 15b). At higher temperature, the solder undergoes large plastic deformation with higher creep rate till the end of the dwell time. The solder fillet, at elevated temperature, owing to its lower yield strength and high creep rate is likely to allow the column tilt toward the direction of global bending as shown in Fig. 15b. On

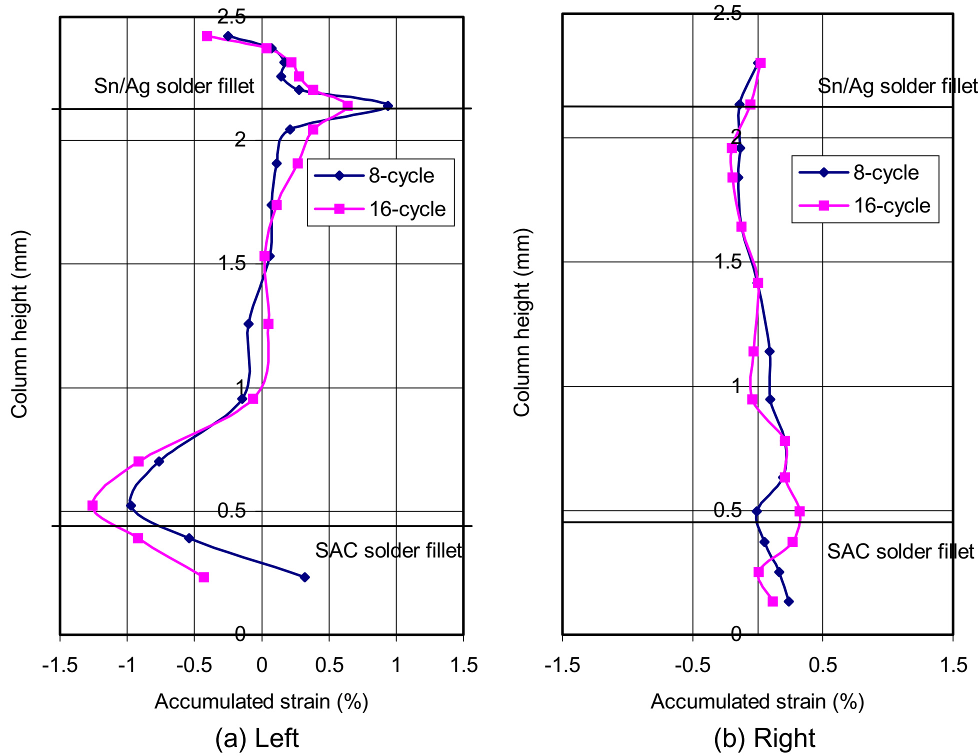

Fig. 14. Accumulated plastic strains during thermal cycles along left and right edges of outermost column.

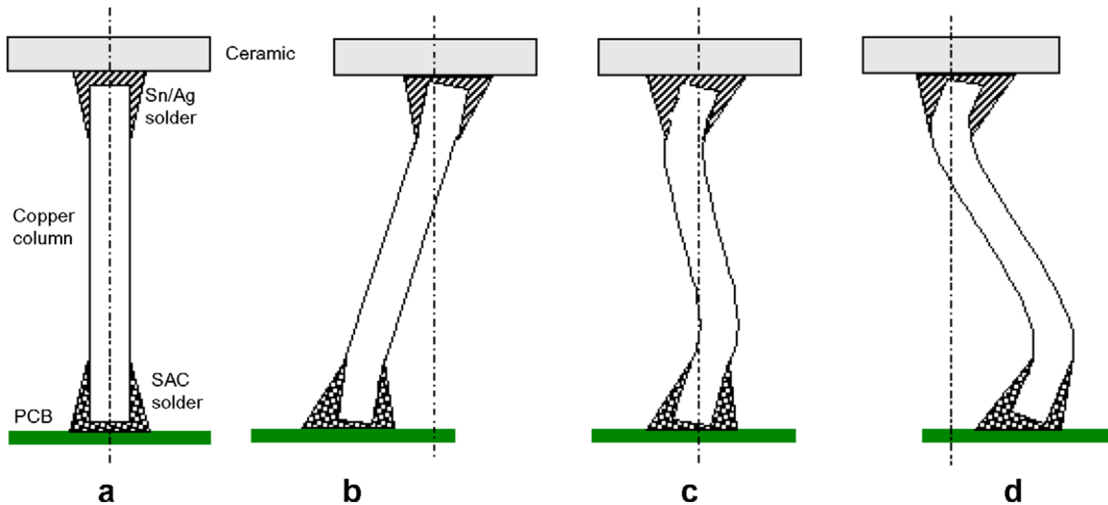

Fig. 15. Schematic diagram of deformation mechanism of outermost column during thermal cycling; (a) at room temp (b) heated to elevated temperature (c) cooled to room temperature and (d) cooled further to lowest temperature.

cooling back to room temperature, all the relative displacement would be recovered. However, the portion of the column enclosed in the solder fillet tries to creep back to regain its original form but it is constrained by the solder fillet. The resulting shape due to this would be that shown in Fig. 15c. However, it does not regain the shape due to the low creep rate at a lower temperature. Further cooling to the lower temperature would cause the lower part of the assembly to contract more than the upper part as illustrated in Fig. 15d. Only the portion of the copper column above the fillets will bend due to the constraints of the solder fillet and the reduced creep behavior. Thus the radius of bending decreases at the fillets resulting in higher bending strains.

It should also be noted that the Pb-free solder of the CuCGA has a higher melting temperature than the eutectic solder of the CCGA. As a result, the eutectic solder creeps more than the Pb-free solder at higher homologous temperatures (i.e. ratio of test temperature to the melting temperature). Therefore at these temperatures, the column

bending at the fillets will be greater in case of tin–lead CCGA than in the CuCGA package.

5. Failure mode

Although the strain analysis suggests similar significant plastic strain at the top of solder fillets in both tin–lead and copper columns in each temperature cycle [4,6,7], the fatigue failure differs for the CuCGA from that typically seen in tin–lead CCGA package.

In the CuCGA, the failure is observed to occur first in the bulk of the solder fillet on the ceramic side along the periphery of the copper column [2]. The crack propagates along the boundary of the copper and solder interface. This is an indication that the fatigue life of the solder in the fillet is less than that of the copper column. In addition, the copper and tin intermetallic is weaker and brittle compared to tin–lead solder [14]. The nature of this failure is unlike that observed for tin–lead columns where the failure occurs at the tin–lead column near the top of the fillet and through the column thickness [6,7]. The CuCGA crack formations are shown in Fig. 16, which are taken at the end of 28 cycles. Separate fatigue failure data compiled from the literature is presented in Table 2 for reference. It can be inferred from the table that the fatigue life of the shorter (1.5 mm) Pb-free CuCGA is comparable to that of the 2.2 mm Sn–Pb CCGA. The thermal cycling test data of the 2.2 mm copper column from [2,13], revealed a higher cycle life for the copper columns. Higher sigma (standard deviation) values indicate process and other constraints of the new setup.

The peripheral crack formation in the CuCGA could also be explained based on the deformation mechanism suggested above. Due to the repeated expansion and contraction of the entire assembly and due to the CTE differences between Cu and solder, there is permanent deformation and localized high compressive strains in the Pb-free solder fillet. The ratcheting action and weakness of the copper/tin intermetallic causes a crack to form in the solder fillet near the solder-column interface, which can rapidly propagate along the interface boundary.

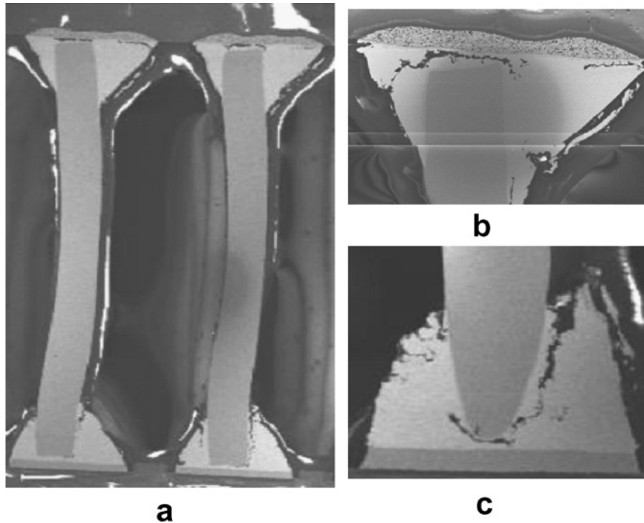

Fig. 16. (a) Typical deformation of high-DNP columns; (b) ceramic-side and (c) board-side column images of the outermost column (2.46 mm long, 0.25 mm diameter) after 28 thermal cycles showing crack initiation along the periphery of the copper column.

6. Conclusion

The thermo-mechanical behavior of the Pb-free CuCGA package (1657 I/O, 42.5 mm size, 2.46 mm × 0.25 mm Cu column dimensions) was studied in comparison with a similar tin–lead CCGA package (1089 I/O, 42.5 mm size, 2.2 mm × 0.57 mm column dimensions) using high sensitivity moiré interferometry. The package was subjected to an isothermal load of $\Delta T = -75$ °C and subsequent accelerated thermal cycles of −40 °C to +125 °C. The analysis indicated that the dominant deformation mode was bending of the column caused by the CTE mismatch between the ceramic module and the PCB. Equivalent amount of global deformation for $\Delta T = -60$ °C between the CuCGA (41 × 41 array) and the CCGA (33 × 33 array) indicated that either both packages had similar global stiffness of

Table 2
Fatigue life data comparison from literature [2,6,13]

Type	Feature	Size (mm)	I/Os (pitch)	Column geometry	Stress condition	Sample size	First fail (cycles)	N50 (cycles)	Sigma
Pb/Sn [6]	Column: 90Pb/10Sn Solder: 63Pb/37Sn	42.5	1089 I/O, 1.27 mm	$l = 2.2$ mm $d = 0.57$ mm	−40 °C to 125 °C, 2 cph	–	1783	–	–
Pb/Sn [13]	Column: 90Pb/10Sn Solder: 63Pb/37Sn	42.5	1089 I/O, 1.27 mm	$l = 2.2$ mm $d = 0.57$ mm	−55 ° to 110 °, 2 cph	51	1500	1760	0.14
Pb/Sn [13]	Column: 90Pb/10Sn Solder: 63Pb/37Sn	42.5	1657 I/O, 1.0 mm	$l = 2.2$ mm $d = 0.57$ mm	0 °C to 100 °C, 3 cph −55 °C to 100 °C, 2 cph	26 35	2485 1000	2820 1253	0.11 0.09
Pb-free [2]	Column: Cu Solder: 82Sn/18Ag Sn/3.9Ag/0.6Cu	42.5	1657 I/O, 1.0 mm	$l = 1.5$ mm $d = 0.25$ mm	0 °C to 100 °C, 2 cph	30	1660	2410	0.26
Pb-free [2]	Column: Cu Solder: 82Sn/18Ag Sn/3.9Ag/0.6Cu	42.5	1657 I/O, 1.0 mm	$l = 2.2$ mm $d = 0.25$ mm	0 °C to 100 °C, 2 cph	–	–	4300	–

the column interconnects or the column stiffness was insignificant relative to the ceramic/PCB moduli. The S-shaped deformation of the column was explained by the solder fillet constraint and creep rate difference of the solder at high and low temperatures. Pb-free solders have higher melting temperatures compared to eutectic Sn–Pb solders. As a result, eutectic Sn–Pb solder creeps more causing greater bending in tin–lead columns. The bending strain distribution revealed that the maximum plastic strain occurred at the top of the solder fillet for both CuCGA and SnPb CCGA. Since copper columns were thinner and taller than the tin–lead columns, the CuCGA accumulated smaller plastic strain per cycle. Accordingly, if we assumed that the fatigue life for the copper and tin–lead columns was the same and the failure occurred at the same location, then a longer life could be expected for the CuCGA package. The fatigue test data reveal a comparable cycle life for the (2.2 mm) Sn–Pb CCGA and the shorter (1.5 mm) Cu column Pb-free CuCGA. However, the fatigue life of the taller (2.2 mm) column CuCGA is far superior to that of the Sn–Pb CCGA of the same column height. In the CuCGA, crack initiates in the solder fillet near the column and solder interface. Plastic deformation associated with thermal cycling, coupled with ratcheting action and weakness of copper/tin intermetallic, causes the crack to propagate along the interface of the solder and copper column.

Further study of the fatigue life characteristics of the copper, tin–lead column and Pb-free solder fillet is suggested to predict more accurately its life cycle in the field.

Acknowledgements

The authors wish to thank Lewis Goldman, Marie Cole, Mario Interrante and Greg Martin of IBM at East Fishkill, who provided the CuCGA samples for analysis and provided valuable technical inputs and advise.

References

[1] Farooq M et al. Thermo-mechanical fatigue reliability of Pb-Free ceramic ball grid arrays: experimental data and lifetime prediction modeling. Proceedings of the 53rd electronic components and technology conference. New Orleans, LA: IEEE; 2003.

[2] Interrante M et al. Lead-free package interconnections for ceramic grid arrays. In: Proceedings of SEMICON/West 2003 international electronics manufacturing technology symposium, Santa Clara, CA; 2003.

[3] Cole M et al. Lead-free card assembly and rework for column grid arrays. J Surface Mount Technol 2004;17(1):33–40.

[4] Perkins A, Sitaraman S. Thermo-mechanical failure comparison and evaluation of CCGA and CBGA electronic packages. In: Proceedings of the 53rd electronics components and technology conference, New Orleans, LA; 2003.

[5] Perkins A, Sitaraman S. Vibration-induced solder joint failure of a ceramic column grid array (CCGA) package. In: Proceedings of the 54th electronics components and technology conference, Las Vegas, NV; 2004.

[6] Han B. Deformation mechanism of two-phase solder column interconnections under highly accelerated thermal cycling condition: an experimental study. J Elect Packag 1997;119:189–96.

[7] Lau JH et al. Reliability testing and data analysis of an 1657CCGA (ceramic column grid array) package with lead-free solder paste on lead-free PCBs (printed circuit boards). In: Proceedings of the 54th electronics components and technology conference, Las Vegas, NV; 2004.

[8] Lau JH, Dauksher W. Reliability of an 1657CCGA (ceramic column grid array) package with 96.5Sn3.9Ag0.6Cu lead-free solder paste on PCBs (printed circuit boards). ASME IMECE2003, Paper No. 44041, 2003

[9] Han B. Optical methods as tools for electronic packaging product development. Adv Packag 1997:44–66. May/June.

[10] Post D, Han B, Ifju P. High sensitivity moire. New York: Springer-Verlag; 1994. p. 65–7, 135–6.

[11] Tra-Bond F253 – Color keyed, high temperature epoxy adhesive, Tra-Bond F114 – Optically clear, low viscosity blush-free epoxy adhesive, Tra-con, Inc. Available from: http://www.tra-con.com/.

[12] Ceramic Column Grid Array – Assembly and Rework User's Guide, 2002, IBM.

[13] C4 CBGA and CCGA Reliability Data, 2000, IBM Unclassified.

[14] Field RJ, Low SR. Physical and mechanical properties of intermetallic compounds commonly found in solder joints. NIST 2001.